ARTICLE IN PRESS

Computational Materials Science xxx (2014) xxx–xxx

Contents lists available at ScienceDirect

Computational Materials Science

journal homepage: www.elsevier.com/locate/commatsci

Analysis of laminated composite plates integrated with piezoelectric sensors and actuators using higher-order shear deformation theory and isogeometric finite elements

P. Phung-Van [a,b], L. De Lorenzis [c], Chien H. Thai [a], M. Abdel-Wahab [b], H. Nguyen-Xuan [d,*]

[a] Division of Computational Mechanics, Ton Duc Thang University, 19 Nguyen Huu Tho, Tan Phong Ward, Dist. 7, HCMC, Viet Nam
[b] Department of Mechanical Construction and Production, Faculty of Engineering and Architecture, Ghent University, Belgium
[c] Institut für Angewandte Mechanik, Technische Universität Braunschweig, Bienroder Weg 87, Campus Nord, 38106 Braunschweig, Germany
[d] Duy Tan University, Da Nang, Viet Nam

ARTICLE INFO

Article history:
Received 18 February 2014
Received in revised form 28 March 2014
Accepted 30 April 2014
Available online xxxx

Keywords:
Composite plates
Smart materials
Vibration
Computational modeling
Isogeometric Analysis (IGA)
Sensors and actuators

ABSTRACT

This paper presents a simple and effective formulation based on Isogeometric Analysis (IGA) and Higher-order Shear Deformation Theory (HSDT) to investigate static, free vibration and dynamic control of piezoelectric composite plates integrated with sensors and actuators. In the composite plates, the mechanical displacement field is approximated according to the HSDT model using isogeometric elements based on Non-Uniform Rational B-Spline (NURBS) basis functions. These achieve naturally any desired degree of continuity through the choice of the interpolation order, so that the method easily fulfills the C^1-continuity requirement of the HSDT model. The electric potential is assumed to vary linearly through the thickness for each piezoelectric sublayer. A displacement and velocity feedback control algorithm is used for the active control of the static deflection and of the dynamic response of the plates through a closed-loop control with bonded or embedded distributed piezoelectric sensors and actuators. The accuracy and reliability of the proposed method is verified by comparing its numerical predictions with those of other available numerical approaches.

1. Introduction

The integration of composite plates with piezoelectric materials to obtain active lightweight smart structures has attracted a considerable interest for various applications such as automotive sensors, actuators, transducers and active damping devices. Piezoelectric materials are often used to design smart structures in industrial, medical, military and scientific areas. One of the essential features of piezoelectric materials is their ability of transformation between mechanical energy and electric energy. Specifically, when piezoelectric materials are deformed, electric charges are generated, and conversely, the application of an electric field produces mechanical deformations in the structure [1].

Due to the attractive properties of piezoelectric composite structures, various numerical methods have been proposed to model and simulate their behavior. For static and free vibration analysis, Yang and Lee [2] showed that the early work on structures with piezoelectric layers, which ignored the mass and stiffness of the layers, could lead to substantial errors in the natural frequencies and mode shapes. Pletner and Abramovich [3] studied a consistent technique for modeling piezolaminated shells. Hong and Chopra [4] incorporated the piezoelectric layers as plies with special properties into the laminate and assumed that consistent deformations exist in the substrate and piezoelectric layers. Kim et al. [5] validated the finite element (FE) model of a smart cantilever plate through comparison with experiments. Willberg and Gabbert [6] studied a three-dimensional piezoelectric solid model using isogeometric finite elements. FE models for piezoelectric composite beams and plates have been reported in Refs. [7–16]. Additionally, several other numerical methods [34–48] are promising to solve various piezoelectric structures.

For vibration control, some theories integrated with various numerical methods have been proposed and can be generally classified into two categories, namely, the analytical methods and the equivalent single-layer theories. In the framework of analytical methods, smart beams with embedded or surface distributed piezoelectric sensors and actuators were initially investigated in Refs. [17,18]. Tzou and Tseng [19] developed a piezoelectric thin hexahedron solid element for analysis of plates and shells with

* Corresponding author. Tel.: +84 0822137144.
E-mail address: nguyenxuanhung@duytan.edu.vn (H. Nguyen-Xuan).

http://dx.doi.org/10.1016/j.commatsci.2014.04.068
0927-0256/

Please cite this article in press as: P. Phung-Van et al., Comput. Mater. Sci. (2014), http://dx.doi.org/10.1016/j.commatsci.2014.04.068

distributed piezoelectric sensors and actuators. The three most popular equivalent single-layer theories are the Classical Lamination Theory (CLT), the First-order Shear Deformation Theory (FSDT), and the Higher-order Shear Deformation Theory (HSDT).

In the CLT, which is based on the assumptions of Kirchhoff's plate theory, the interlaminar shear deformation is neglected. Following this framework, Hwang and Park [20] and Lam et al. [7] introduced control algorithms based on classical negative velocity feedback control and the FE method which were formulated based on the discrete Kirchhoff quadrilateral element or the rectangular plate bending element. Liu et al. [21,22] studied the active vibration control of beams and plates containing distributed sensors and actuators. In these works, the formulation of vibration control simulation was based on the classical plate theory and the Radial Point Interpolation Method (RPIM).

In the FSDT, a constant transverse shear deformation is assumed through the entire thickness of the laminate and hence stress-free boundary conditions are violated at the top and bottom surfaces of the panel. Using this theory, Liew et al. [23] applied the element-free Galerkin method to laminated composite beams and plates with piezoelectric patches. Milazzo and Orlando [24] studied free vibration analysis of smart laminated thick composite plates. Phung-Van et al. [25] extended the cell-based smoothed discrete shear gap method to static, free vibration and control of piezoelectric composite plates. Some FE formulations based on FSDT for analysis of smart laminated plates and shells were studied in Refs. [26–28].

In both CLT and FSDT theories, a shear correction factor is required to ensure the stability of the solution. In order to improve the accuracy of transverse shear stresses and to avoid the introduction of shear correction factors, the HSDT based on the FE method has been proposed to study piezoelectric plates [29–31]. In this theory, quadratic, cubic or higher-order variations of surface-parallel displacements are assumed through the entire thickness of the piezoelectric composite plate to model the behavior of the structure. It is worth mentioning that the HSDT requires at least C^1-continuity of generalized displacements due to the presence of their second-order derivatives in the stiffness formulation. This is a source of difficulty in standard finite elements featuring C^0 inter-element continuity.

This paper aims at further contributing to the dynamic analysis of piezoelectric composite plates using an isogeometric approach based on Non-Uniform B-Spline (NURBS) basis functions. In particular, we show that a HSDT formulation fulfilling C^1-continuity requirements is easily achieved in the framework of isogeometric analysis.

Isogeometric Analysis (IGA) has been recently proposed by Hughes et al. [32–34] with the original objective to tightly integrate Computer Aided Design (CAD) and FE analysis. IGA makes use of the same basis functions typically used in the CAD environment (most notably NURBS or T-Splines) to describe the geometry of the problem exactly as it is produced from CAD as well as to approximate the solution fields for the analysis. In addition to fulfill the original goal, isogeometric basis functions have been shown to deliver significant advantages for the analysis, independently from the integration with CAD. One of their most notable features is that they can achieve any desired degree of smoothness through the choice of the interpolation order, as opposed to traditional FEM where C^0 inter-element continuity is normally achieved. If p is the order of the discretization, C^{p-1} inter-element continuity is achieved when no repeated entries in the knot vectors are present. Hence, IGA easily fulfills the C^1-continuity requirements for plate elements stemming from the HSDT, which is of interest in this study. In the past few years, IGA has been successfully applied to various fields and achieves the high accuracy compared to the exact solutions. Particularly, the advantages of IGA reported in the recent investigations [49–58] on plate and shell structures are of our great motivation for analysis of piezoelectric structures.

This paper exploits further the advantages of a NURBS-based isogeometric approach for static, free vibration and dynamic control analysis of laminated composite plates integrated with piezoelectric sensors and actuators using the HSDT theory. In the piezoelectric composite plates, the mechanical displacement field is approximated according to the HSDT model using C^1-continuous NURBS isogeometric elements. Thus the C^1-continuity requirement is naturally achieved by choosing at least a quadratic interpolation with no repeated knot vector entries. The electric potential is assumed to vary linearly through the thickness for each piezoelectric sublayer. A displacement and velocity feedback algorithm is used for active control of the static deflection and of the dynamic response of the plates, through a closed-loop control with bonded or embedded distributed piezoelectric sensors and actuators. The accuracy and reliability of the method is verified by comparing its numerical predictions with those of other available numerical approaches.

2. Governing equations and weak form for piezoelectric composite plates

In this section, the governing equations for piezoelectric composite plates are presented and the weak form is established via a classical variational formulation [8,9]. Fig. 1 shows the geometry of a piezoelectric composite plate. The layers are assumed to be perfectly bonded, elastic and orthotropic [10] with small strains and displacements [11], and the deformation is taking place under isothermal conditions. In addition, the piezoelectric sensors and actuators are made of homogenous and isotropic dielectric materials [12] and high electric fields as well as cyclic fields are excluded [13]. Based on these assumptions, a linear constitutive relationship [14] can be employed for the static and dynamic analysis of the piezoelectric composite plates.

2.1. Linear piezoelectric constitutive equations

The linear piezoelectric constitutive equations can be expressed as [15,25]

$$\begin{bmatrix} \boldsymbol{\sigma} \\ \mathbf{D} \end{bmatrix} = \begin{bmatrix} \mathbf{c} & -\mathbf{e}^T \\ \mathbf{e} & \mathbf{g} \end{bmatrix} \begin{bmatrix} \boldsymbol{\varepsilon} \\ \mathbf{E} \end{bmatrix} \tag{1}$$

where $\boldsymbol{\sigma}$ and $\boldsymbol{\varepsilon}$ are the stress and strain vectors; $\mathbf{D}$ and $\mathbf{E}$ are the dielectric displacement and electric field vectors; $\mathbf{c}$ is the elasticity

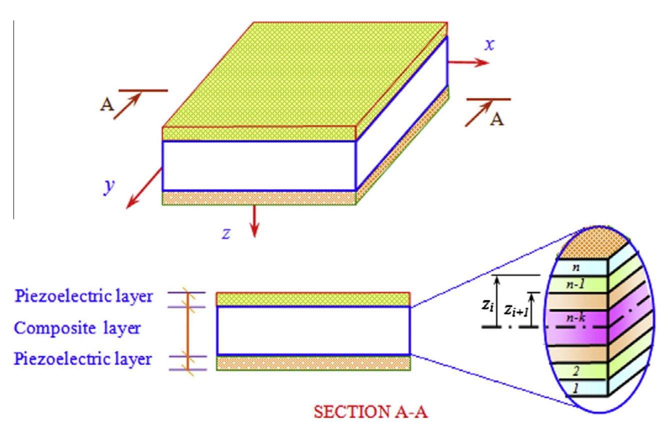

Fig. 1. Configuration of a piezoelectric laminated composite plate.

matrix given in Section 2.3.1; $\mathbf{e}$ is the piezoelectric constant matrix and $\mathbf{g}$ denotes the dielectric constant matrix given in Section 2.4.

In addition, the electric field vector $\mathbf{E}$ is related to the gradient of the electric potential field ϕ [19] as follows

$$\mathbf{E} = -\text{grad } \phi \tag{2}$$

2.2. Weak form for piezoelectric composite plates

The weak form of the governing equations for piezoelectric structures can be derived by using Hamilton's variational principle [20] which can be written as

$$\delta L = 0 \tag{3}$$

where L is the general energy functional which contains the summation of kinetic energy, strain energy, dielectric energy and external work and is written in the following form

$$L = \int_{\Omega}\left(\frac{1}{2}\rho\dot{\mathbf{u}}^T\dot{\mathbf{u}} - \frac{1}{2}\boldsymbol{\sigma}^T\varepsilon + \frac{1}{2}\mathbf{D}^T\mathbf{E} + \mathrm{uf}_s - \boldsymbol{\phi}\mathbf{q}_s\right)\mathrm{d}\Omega + \sum \mathbf{u}^T\mathbf{F}_p - \sum \boldsymbol{\phi}\mathbf{Q}_p \tag{4}$$

where ρ is the mass density, $\mathbf{u}$ and $\dot{\mathbf{u}}$ are the mechanical displacement and velocity; $\boldsymbol{\phi}$ is the electric potential; $\mathbf{f}_s$ and $\mathbf{F}_p$ are the mechanical surface loads and point loads; $\mathbf{q}_s$ and $\mathbf{Q}_p$ are the surface charges and point charges.

In the variational form of Eq. (3), the mechanical displacement field $\mathbf{u}$ and the electric potential field $\boldsymbol{\phi}$ are the unknown functions. To solve for these unknowns numerically, it is necessary to choose a suitable approximation for the mechanical displacement field and the electric potential field. In the present work, isogeometric finite elements are used to approximate the mechanical displacement field of piezoelectric composite plates. Due to the above assumptions leading to a linear constitutive relationship [14], the formulation for each field can be defined separately.

2.3. Approximation of the mechanical displacement field

2.3.1. Governing equations for a third-order shear deformation theory model

According to the third-order shear deformation theory proposed by Reddy [59], the displacements of an arbitrary point in the plate are expressed by

$$\begin{aligned} u(x,y,z) &= u_0 + z\beta_x + cz^3(\beta_x + w_{,x}) \\ v(x,y,z) &= v_0 + z\beta_y + cz^3(\beta_y + w_{,y}), \quad (-t/2 \leqslant z \leqslant t/2) \\ w(x,y,z) &= w_0 \end{aligned} \tag{5}$$

where t is the thickness of the plate; $c = 4/3t^2$ and the variables $\mathbf{u}_0 = [u_0\ v_0]^T$, w_0 and $\boldsymbol{\beta} = [\beta_x\ \beta_y]^T$ are the membrane displacements, the deflection of the mid-plane and the rotations of the mid-plane around y-axis and x-axis, respectively.

The in-plane strains are thus expressed by the following equation

$$\boldsymbol{\varepsilon} = [\varepsilon_{xx}\ \varepsilon_{yy}\ \gamma_{xy}]^T = \boldsymbol{\varepsilon}_0 + z\boldsymbol{\kappa}_1 + z^3\boldsymbol{\kappa}_2 \tag{6}$$

where

$$\boldsymbol{\varepsilon}_0 = \begin{bmatrix} u_{0,x} \\ v_{0,y} \\ u_{0,y} + v_{0,x} \end{bmatrix}, \quad \boldsymbol{\kappa}_1 = \begin{bmatrix} \beta_{x,x} \\ \beta_{y,y} \\ \beta_{x,y} + \beta_{y,x} \end{bmatrix}, \quad \boldsymbol{\kappa}_2 = c\begin{bmatrix} \beta_{x,x} + w_{0,xx} \\ \beta_{y,y} + w_{0,yy} \\ \beta_{x,y} + \beta_{y,x} + 2w_{0,xy} \end{bmatrix} \tag{7}$$

and the transverse shear strains are given by

$$\boldsymbol{\gamma} = [\gamma_{xz} \quad \gamma_{yz}]^T = \boldsymbol{\varepsilon}_s + z^2\boldsymbol{\kappa}_s \tag{8}$$

with

$$\boldsymbol{\varepsilon}_s = \begin{bmatrix} \beta_x + w_{0,x} \\ \beta_y + w_{0,y} \end{bmatrix}, \quad \boldsymbol{\kappa}_s = 3c\begin{bmatrix} \beta_x + w_{0,x} \\ \beta_y + w_{0,y} \end{bmatrix} \tag{9}$$

In the laminated composite plate, the constitutive equation of the kth orthotropic layer in local coordinates is derived from Hooke's law for plane stress as

$$\begin{Bmatrix} \sigma_{xx} \\ \sigma_{yy} \\ \tau_{xy} \\ \tau_{xz} \\ \tau_{yz} \end{Bmatrix}^{(k)} = \begin{bmatrix} Q_{11} & Q_{12} & Q_{16} & 0 & 0 \\ Q_{21} & Q_{22} & Q_{26} & 0 & 0 \\ Q_{61} & Q_{62} & Q_{66} & 0 & 0 \\ 0 & 0 & 0 & Q_{55} & Q_{54} \\ 0 & 0 & 0 & Q_{45} & Q_{44} \end{bmatrix}^{(k)} \begin{Bmatrix} \varepsilon_{xx} \\ \varepsilon_{yy} \\ \gamma_{xy} \\ \gamma_{xz} \\ \gamma_{yz} \end{Bmatrix}^{(k)} \tag{10}$$

where the material constants are given by

$$\begin{aligned} &Q_{11} = \frac{E_1}{1 - \nu_{12}\nu_{21}}, \quad Q_{12} = \frac{\nu_{12}E_2}{1 - \nu_{12}\nu_{21}}, \quad Q_{22} = \frac{E_2}{1 - \nu_{12}\nu_{21}} \\ &Q_{66} = G_{12}, \quad Q_{55} = G_{13}, \quad Q_{44} = G_{23} \end{aligned} \tag{11}$$

in which E_1, E_2 are the Young moduli in the x and y directions, respectively, G_{12}, G_{23}, G_{13} are the shear moduli in the $x-y$, $y-z$, $z-x$ planes, respectively, and ν_{ij} are the Poisson's ratios.

The laminate is usually made of several orthotropic layers with differently oriented orthotropy directions. The stress–strain relation for the kth orthotropic lamina (with arbitrary fiber orientation compared to the reference axes) in the global reference system is computed by

$$\begin{Bmatrix} \sigma_{xx} \\ \sigma_{yy} \\ \tau_{xy} \\ \tau_{xz} \\ \tau_{yz} \end{Bmatrix}^{(k)} = \begin{bmatrix} \overline{Q}_{11} & \overline{Q}_{12} & \overline{Q}_{16} & 0 & 0 \\ \overline{Q}_{21} & \overline{Q}_{22} & \overline{Q}_{26} & 0 & 0 \\ \overline{Q}_{61} & \overline{Q}_{62} & \overline{Q}_{66} & 0 & 0 \\ 0 & 0 & 0 & \overline{Q}_{55} & \overline{Q}_{54} \\ 0 & 0 & 0 & \overline{Q}_{45} & \overline{Q}_{44} \end{bmatrix}^{(k)} \begin{Bmatrix} \varepsilon_{xx} \\ \varepsilon_{yy} \\ \gamma_{xy} \\ \gamma_{xz} \\ \gamma_{yz} \end{Bmatrix}^{(k)} \tag{12}$$

where $\overline{Q}_{ij}$ are the transformed material constants of the kth lamina [60].

From Hooke's law and the linear strains given by Eqs. (6) and (8), the stress is computed by

$$\boldsymbol{\sigma} = \begin{bmatrix} \boldsymbol{\sigma}_p \\ \boldsymbol{\tau} \end{bmatrix} = \underbrace{\begin{bmatrix} \overline{\mathbf{D}} & \mathbf{0} \\ \mathbf{0} & \overline{\mathbf{D}}_s \end{bmatrix}}_{\mathbf{c}} \underbrace{\begin{bmatrix} \boldsymbol{\varepsilon} \\ \boldsymbol{\gamma} \end{bmatrix}}_{\boldsymbol{\varepsilon}} = \mathbf{c}\boldsymbol{\varepsilon} \tag{13}$$

where $\boldsymbol{\sigma}_p$ and $\boldsymbol{\tau}$ are the in-plane stress component and shear stress; $\overline{\mathbf{D}}$ and $\overline{\mathbf{D}}_s$ are material constant matrices given in the form of

$$\overline{\mathbf{D}} = \begin{bmatrix} \mathbf{A} & \mathbf{B} & \mathbf{E} \\ \mathbf{B} & \mathbf{D} & \mathbf{F} \\ \mathbf{E} & \mathbf{F} & \mathbf{H} \end{bmatrix}, \quad \overline{\mathbf{D}}_\mathbf{s} = \begin{bmatrix} \mathbf{A}_s & \mathbf{B}_s \\ \mathbf{B}_s & \mathbf{D}_s \end{bmatrix} \tag{14}$$

in which

$$\begin{aligned} (\mathbf{A}, \mathbf{B}, \mathbf{D}, \mathbf{E}, \mathbf{F}, \mathbf{H}) &= \int_{-h/2}^{h/2} (1, z, z^2, z^3, z^4, z^6)\overline{Q}_{ij}\,\mathrm{d}z \quad i,j = 1,2,6 \\ (\mathbf{A}_s, \mathbf{B}_s, \mathbf{D}_s) &= \int_{-h/2}^{h/2} (1, z^2, z^4)\overline{Q}_{ij}\,\mathrm{d}z \quad i,j = 4,5 \end{aligned} \tag{15}$$

2.3.2. A C^1-continuous isogeometric composite plate formulation based on HDST

2.3.2.1. A brief review of NURBS basis functions. A knot vector $\boldsymbol{\Xi} = \{\xi_1, \xi_2, \ldots, \xi_{n+p+1}\}$ is defined as a sequence of knot values $\xi_i \in R$, $i = 1, \ldots, n+p+1$. If the first and the last knots are repeated $p+1$ times, the knot vector is called open. A B-spline basis function is C^∞ continuous inside a knot span and C^{p-1} continuous at each unique knot. Each repetition of a knot decreases by one the degree of continuity at the knot.

The univariate B-spline basis functions $N_{i,p}(\xi)$ are defined by the Cox–De Boor recursive formula

$$N_{i,p}(\xi) = \frac{\xi - \xi_i}{\xi_{i+p} - \xi_i} N_{i,p-1}(\xi) + \frac{\xi_{i+p+1} - \xi}{\xi_{i+p+1} - \xi_{i+1}} N_{i+1,p-1}(\xi)$$
$$\text{as } p = 0,\ N_{i,0}(\xi) = \begin{Bmatrix} 1 & \text{if } \xi_i \leqslant \xi < \xi_{i+1} \\ 0 & \text{otherwise} \end{Bmatrix} \tag{16}$$

Bivariate B-spline basis functions are obtained as the tensor product of univariate basis functions in two parametric dimensions ξ and η associated to two knot vectors $\boldsymbol{\Xi} = \{\xi_1, \xi_2, \ldots, \xi_{n+p+1}\}$ and $\mathbf{H} = \{\eta_1, \eta_2, \ldots, \eta_{m+q+1}\}$,

$$N_I^b(\xi,\eta) = N_{i,p}(\xi) M_{j,q}(\eta) \tag{17}$$

To present exactly some curved geometries (e.g. conics) the NURBS functions are used. Differently from the B-spline case, each NURBS control point is associated to an additional value called weight ζ_I [32]. Then the NURBS functions can be expressed as

$$N_I(\xi,\eta) = \frac{N_I^b \zeta_I}{\sum_A^{m\times n} N_A^b(\xi,\eta)\zeta_A} \tag{18}$$

It is clear that B-spline functions are a special case of NURBS functions obtained when the individual weights of all control points are equal.

It is obvious that for $p = 0$ or 1 the NURBS basis functions are identical to those of standard piecewise constant and linear finite elements, respectively. They are different for $p \geqslant 2$ and importantly the present approach easily satisfies the C^1 continuity requirement stemming from the third-order shear deformation theory.

2.3.2.2. NURBS-based novel composite plate formulation. Using the NURBS basis functions above, the displacement field $\mathbf{u}$ of the plate is approximated as

$$\mathbf{u}^h(\xi,\eta) = \sum_I^{m\times n} N_I(\xi,\eta)\mathbf{d}_I \tag{19}$$

where $\mathbf{d}_I = [u_{0I}\ v_{0I}\ w_{0I}\ \beta_{xI}\ \beta_{xI}]^T$ is the vector of degrees of freedom associated with the control point I.

Substituting Eq. (19) into Eqs. (6) and (8), the in-plane and shear strains can be rewritten as:

$$\begin{aligned}&\begin{bmatrix} \boldsymbol{\varepsilon}_0^T & \boldsymbol{\kappa}_1^T & \boldsymbol{\kappa}_2^T & \boldsymbol{\varepsilon}_s^T & \boldsymbol{\kappa}_s^T \end{bmatrix}^T \\ &= \sum_{A=1}^{m\times n} \begin{bmatrix} \left(\mathbf{B}_I^m\right)^T & \left(\mathbf{B}_I^{b1}\right)^T & \left(\mathbf{B}_I^{b2}\right)^T & \left(\mathbf{B}_I^{s0}\right)^T & \left(\mathbf{B}_I^{s1}\right)^T \end{bmatrix}^T \mathbf{d}_I\end{aligned} \tag{20}$$

where

$$\mathbf{B}_I^m = \begin{bmatrix} N_{I,x} & 0 & 0 & 0 & 0 \\ 0 & N_{I,y} & 0 & 0 & 0 \\ N_{I,y} & N_{I,x} & 0 & 0 & 0 \end{bmatrix}, \quad \mathbf{B}_I^{b1} = \begin{bmatrix} 0 & 0 & 0 & N_{I,x} & 0 \\ 0 & 0 & 0 & 0 & N_{I,y} \\ 0 & 0 & 0 & N_{I,y} & N_{I,x} \end{bmatrix},$$
$$\mathbf{B}_I^{b2} = c\begin{bmatrix} 0 & 0 & N_{I,xx} & N_{I,x} & 0 \\ 0 & 0 & N_{I,yy} & 0 & N_{I,y} \\ 0 & 0 & 2N_{I,xy} & N_{I,y} & N_{I,x} \end{bmatrix}, \quad \mathbf{B}_I^{s0} = \begin{bmatrix} 0 & 0 & N_{I,x} & N_I & 0 \\ 0 & 0 & N_{I,y} & 0 & N_I \end{bmatrix},$$
$$\mathbf{B}_I^{s1} = 3c\begin{bmatrix} 0 & 0 & N_{I,x} & N_I & 0 \\ 0 & 0 & N_{I,y} & 0 & N_I \end{bmatrix} \tag{21}$$

2.4. Approximation of the electric potential field

In the present study, the electric potential field of each piezoelectric layer is approximated by discretizing each piezoelectric layer into finite sub-layers along the thickness direction. In each sublayer, a linear electric potential function is assumed through the thickness as [11]

$$\phi^i(z) = \mathbf{N}_\phi^i \boldsymbol{\phi}^i \tag{22}$$

where $\mathbf{N}_\phi^i$ is the vector of the shape functions for the electric potential, defined through Eqs. (16) and (17) with $p = 1$, and $\boldsymbol{\phi}^i$ is the vector containing the electric potentials at the top and bottom surfaces of the i-th sublayer, $\boldsymbol{\phi}^i = \begin{bmatrix} \phi^{i-1} & \phi^i \end{bmatrix}$ $(i = 1, 2, \ldots, n_{sub})$ in which n_{sub} is the number of piezoelectric layers.

For each piezoelectric sublayer element, it is assumed that values of electric potentials at the same height along the thickness are as defined in [15,20]. Hence, for each sub-layer element, the electric field $\mathbf{E}$ in Eq. (2) can be rewritten as

$$\mathbf{E} = -\nabla \mathbf{N}_\phi^i \boldsymbol{\phi}^i = -\mathbf{B}_\phi \boldsymbol{\phi}^i \tag{23}$$

Note that, for the type of piezoelectric materials considered in this work the piezoelectric constant matrix $\mathbf{e}$ and the dielectric constant matrix $\mathbf{g}$ of the kth orthotropic layer in the local coordinate system read [11]

$$\mathbf{e}^{(k)} = \begin{bmatrix} 0 & 0 & 0 & 0 & d_{15} & 0 \\ 0 & 0 & 0 & d_{15} & 0 & 0 \\ d_{31} & d_{32} & d_{33} & 0 & 0 & 0 \end{bmatrix}^{(k)}; \quad \mathbf{g}^{(k)} = \begin{bmatrix} p_{11} & 0 & 0 \\ 0 & p_{22} & 0 \\ 0 & 0 & p_{33} \end{bmatrix}^{(k)} \tag{24}$$

In addition, the laminate is usually made of several orthotropic layers with different directions of orthotropy and consequently different characteristic directions for the dielectric and piezoelectric properties. The piezoelectric constant matrix for the kth orthotropic lamina in the global coordinate system is given by

$$\mathbf{e}^{(k)} = \begin{bmatrix} 0 & 0 & 0 & 0 & \bar{d}_{15} & 0 \\ 0 & 0 & 0 & \bar{d}_{15} & 0 & 0 \\ \bar{d}_{31} & \bar{d}_{32} & \bar{d}_{33} & 0 & 0 & 0 \end{bmatrix}^{(k)}; \quad \mathbf{g}^{(k)} = \begin{bmatrix} \bar{p}_{11} & 0 & 0 \\ 0 & \bar{p}_{22} & 0 \\ 0 & 0 & \bar{p}_{33} \end{bmatrix}^{(k)} \tag{25}$$

where $\bar{d}_{ij}$ and $\bar{p}_{ii}$ are transformed material constants of the kth lamina and are calculated similar to $\overline{Q}_{ij}$ in Eq. (12).

2.5. Elementary governing equation of motion

The elementary governing equation of motion can be derived by substituting Eqs. (13), (22) and (23) into Eq. (4), and assembling the electric potentials along the thickness. The final form of this equation is then written in the following form

$$\begin{bmatrix} \mathbf{M}_{uu} & 0 \\ 0 & 0 \end{bmatrix} \begin{bmatrix} \ddot{\mathbf{d}} \\ \ddot{\boldsymbol{\phi}} \end{bmatrix} + \begin{bmatrix} \mathbf{K}_{uu} & \mathbf{K}_{u\phi} \\ \mathbf{K}_{\phi u} & \mathbf{K}_{\phi\phi} \end{bmatrix} \begin{bmatrix} \mathbf{d} \\ \boldsymbol{\phi} \end{bmatrix} = \begin{bmatrix} \mathbf{F} \\ \mathbf{Q} \end{bmatrix} \tag{26}$$

where

$$\begin{aligned}&\mathbf{K}_{uu} = \int_\Omega \mathbf{B}_u^T \mathbf{c} \mathbf{B}_u \mathrm{d}\Omega; \quad \mathbf{K}_{u\phi} = \int_\Omega \mathbf{B}_u^T \mathbf{e}^T \mathbf{B}_\phi \,\mathrm{d}\Omega \\ &\mathbf{K}_{\phi\phi} = -\int_\Omega \mathbf{B}_\phi^T \mathbf{p} \mathbf{B}_\phi \,\mathrm{d}\Omega; \quad \mathbf{M}_{uu} = \int_\Omega \widetilde{\mathbf{N}}^T m \widetilde{\mathbf{N}} \mathrm{d}\Omega\end{aligned} \tag{27}$$

in which $\mathbf{B}_u = [\mathbf{B}^m\ \mathbf{B}^{b1}\ \mathbf{B}^{b2}\ \mathbf{B}^{s0}\ \mathbf{B}^{s1}]^T$; $\mathbf{m}$ is defined by

$$\mathbf{m} = \begin{bmatrix} \mathbf{I}_0 & 0 & 0 \\ 0 & \mathbf{I}_0 & 0 \\ 0 & 0 & \mathbf{I}_0 \end{bmatrix} \text{ where } \mathbf{I}_0 = \begin{bmatrix} I_1 & I_2 & cI_4 \\ I_2 & I_3 & cI_5 \\ cI_4 & cI_5 & c^2 I_7 \end{bmatrix}$$
$$(I_1, I_2, I_3, I_4, I_5, I_7) = \int_{-h/2}^{h/2} \rho(1, z, z^2, z^3, z^4, z^7)\,\mathrm{d}z \tag{28}$$

and

$$\widetilde{\mathbf{N}} = \begin{Bmatrix} \mathbf{N}_1 \\ \mathbf{N}_2 \\ \mathbf{N}_3 \end{Bmatrix}, \quad \mathbf{N}_1 = \begin{bmatrix} N_I & 0 & 0 & 0 & 0 \\ 0 & N_I & 0 & 0 & 0 \\ 0 & 0 & N_I & 0 & 0 \end{bmatrix},$$
$$\mathbf{N}_2 = \begin{bmatrix} 0 & 0 & 0 & N_I & 0 \\ 0 & 0 & 0 & 0 & N_I \\ 0 & 0 & 0 & 0 & 0 \end{bmatrix}, \quad \mathbf{N}_3 = \begin{bmatrix} 0 & 0 & N_{I,x} & N_I & 0 \\ 0 & 0 & N_{I,y} & 0 & N_I \\ 0 & 0 & 0 & 0 & 0 \end{bmatrix} \tag{29}$$

Substituting the second line of Eq. (26) into the first line, we obtain the shortened form as

$$\mathbf{M}\ddot{\mathbf{d}} + \left(\mathbf{K}_{uu} + \mathbf{K}_{u\phi}\mathbf{K}_{\phi\phi}^{-1}\mathbf{K}_{\phi u}\right)\mathbf{d} = \mathbf{F} + \mathbf{K}_{u\phi}\mathbf{K}_{\phi\phi}^{-1}\mathbf{Q} \tag{30}$$

3. Active control analysis

We now consider a piezoelectric laminated composite plate with n ($n \geqslant 2$) layers, as shown in Fig. 2. The top layer is a piezoelectric actuator, denoted with the subscript a, and the bottom layer is a piezoelectric sensor, labeled with the subscript s. In this work, the displacement feedback control [15], which helps to generate the charge by the piezoelectric actuator, is combined with the velocity feedback control [17–22] which can give the velocity component by using an appropriate electronic circuit. In addition, the consistent method [4,21] which can predict the dynamic responses of smart piezoelectric composite plates is adopted. The constant gains G_d and G_v of the displacement feedback control and velocity feedback control [21] are hence used to couple the input actuator voltage vector $\boldsymbol{\phi}_a$ and the output sensor voltage vector $\boldsymbol{\phi}_s$ as

$$\boldsymbol{\phi}_a = G_d\boldsymbol{\phi}_s + G_v\dot{\boldsymbol{\phi}}_s \tag{31}$$

Without the external charge $\mathbf{Q}$, the generated potential on the sensor layer can be derived from the second equation of Eq. (26) as

$$\boldsymbol{\phi}_s = [\mathbf{K}_{\phi\phi}^{-1}]_s[\mathbf{K}_{\phi u}]_s\mathbf{d}_s \tag{32}$$

which implies that, when the plate is deformed by an external force, the electric charges are generated in the sensor layer and are amplified through the closed loop control to be converted into the signal. The converted signal is then sent to the distributed actuator and an input voltage for the actuators is generated. Finally, a resultant force arises through the converse piezoelectric effect and actively controls the static response of the laminated composite plate.

The magnitude of the voltage is defined by substituting Eqs. (31) and (32) into the second equation of Eq. (26) as

$$\mathbf{Q}_a = [\mathbf{K}_{uu}]_a\mathbf{d}_a - G_d[\mathbf{K}_{\phi\phi}]_a[\mathbf{K}_{\phi\phi}^{-1}]_s[\mathbf{K}_{\phi u}]_s\mathbf{d}_s - G_v[\mathbf{K}_{\phi\phi}]_a[\mathbf{K}_{\phi\phi}^{-1}]_s[\mathbf{K}_{\phi u}]_s\dot{\mathbf{d}}_s \tag{33}$$

Substituting Eqs. (32) and (33) into Eq. (30), one writes

$$\mathbf{M}\ddot{\mathbf{d}} + \mathbf{C}\dot{\mathbf{d}} + \mathbf{K}^*\mathbf{d} = \mathbf{F} \tag{34}$$

where

$$\mathbf{K}^* = \mathbf{K}_{uu} + G_d[\mathbf{K}_{u\phi}]_s[\mathbf{K}_{\phi\phi}^{-1}]_s[\mathbf{K}_{\phi u}]_s \tag{35}$$

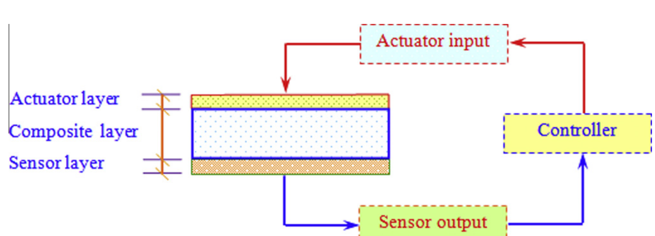

Fig. 2. A schematic diagram of a laminated plate with integrated piezoelectric sensors and actuators.

and $\mathbf{C}$ is the active damping matrix computed by

$$\mathbf{C} = G_v[\mathbf{K}_{u\phi}]_a\left[\mathbf{K}_{\phi\phi}^{-1}\right]_s[\mathbf{K}_{\phi u}]_s \tag{36}$$

If the structural damping effect is considered, Eq. (34) can be rewritten as

$$\mathbf{M}\ddot{\mathbf{d}} + (\mathbf{C} + \mathbf{C}_R)\dot{\mathbf{d}} + \mathbf{K}^*\mathbf{d} = \mathbf{F} \tag{37}$$

where $\mathbf{C}_R$ is the Rayleigh damping matrix assumed to be a linear combination of $\mathbf{M}$ and $\mathbf{K}_{uu}$

$$\mathbf{C}_R = \alpha\mathbf{M} + \beta\mathbf{K}_{uu} \tag{38}$$

in which α and β are the Rayleigh damping coefficients.

For static analyses, Eq. (34) reduces to

$$\mathbf{K}^*\mathbf{d} = \mathbf{F} \tag{39}$$

4. Numerical results

In this section, various numerical examples are performed to demonstrate the accuracy and stability of the isogeometric formulation proposed herein in comparison with some previously adopted approaches. We first demonstrate the accuracy of the IGA solution for the static and free vibration problems. We then demonstrate the performance of the proposed method for the dynamic control of plates integrated with piezoelectric sensors and actuators. The properties of the piezoelectric composite plates, including elastic properties, mass density, piezoelectric coefficients and electric permittivities are given in Table 1. Note that the properties 1, 2 and 3 in Table 1 refer to the directions of axes x,y and z, respectively.

4.1. Free vibration analysis of piezoelectric composite plates

In this section, we investigate the accuracy and efficiency of the proposed isogeometric element for analyzing the natural frequencies of the piezoelectric composite plates. We first consider a square five-ply piezoelectric laminated composite plate [*pie*/0/90/0/*pie*] in which *pie* denotes a piezoelectric layer (see Fig. 3). The plate is simply supported and the thickness to length ratio of each composite ply is $t/a = 1/50$. The laminate configuration includes three layers of Graphite/Epoxy (*Gp*/*Ep*) with fiber orientations of [0/90/0]. Two continuous PZT-4 piezoelectric layers of thickness

Table 1
Material properties of piezoelectric and composite materials.

Properties	PVDF	PZT-4	PZT-G1195N	T300/979	*Gr*/*Ep*
Elastic properties					
E_{11} (GPa)	2	81.3	63.0	150	132.38
E_{22} (GPa)	2	81.3	63.0	9.0	10.76
E_{33} (GPa)	2	64.5	63.0	9.0	10.76
G_{12} (GPa)	1	30.6	24.2	7.1	3.61
G_{13} (GPa)	1	25.6	24.2	7.1	5.65
G_{23} (GPa)	1	25.6	24.2	2.5	5.65
ν_{11}	0.29	0.33	0.30	0.3	0.24
ν_{23}	0.29	0.43	0.30	0.3	0.24
ν_{13}	0.29	0.43	0.30	0.3	0.49
Mass density					
ρ (kg/m^3)	1800	7600	7600	1600	1578
Piezoelectric coefficients					
$d_{31} = d_{32}$ (m/V)	0.046	−1.22e−10	2.54e−10	–	–
d_{15} (m/V)	–	–	–	–	–
Electric permittivities					
p_{11} (F/m)	0.1062e−9	1475	15.3e−9	–	–
p_{22} (F/m)	0.1062e−9	1475	15.3e−9	–	–
p_{33} (F/m)	0.1062e−9	1300	15.0e−9	–	–

Please cite this article in press as: P. Phung-Van et al., Comput. Mater. Sci. (2014), http://dx.doi.org/10.1016/j.commatsci.2014.04.068

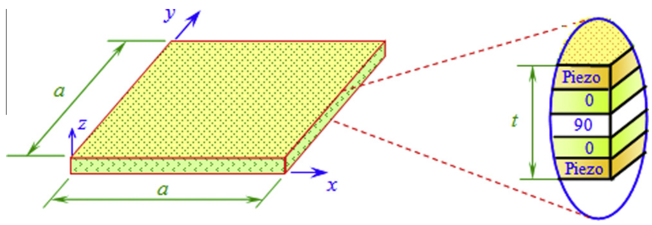

Fig. 3. Model of a 5-ply piezoelectric composite plate.

0.1t are bonded to the upper and lower surfaces of the laminate. Two sets of electric boundary conditions are considered for the inner surfaces of the piezoelectric layers including: (1) a closed-circuit condition in which the electric potential is kept zero (grounded); and (2) an open-circuit condition in which the electric potential remains free (zero electric displacements). The analytical approach [62] to this problem was only available for the first natural frequency and several FE formulations [29,61] were then adopted to obtain other natural frequencies.

Table 2 shows the dimensionless first natural frequency of the piezoelectric composite plate with meshing of 8 × 8 quadratic (p = 2), cubic (p = 3) and quartic (p = 4) elements. The dimensionless first natural frequency is defined as $\bar{f} = \omega_1 a^2/(1000t\sqrt{\rho})$, where ω_1 is the first natural frequency. In this study, the isogeometric elements use the HSDT with only 5 dofs per control point while Ref. [61] uses the layerwise theory and Ref. [29] uses HSDT with 11 dofs per node. It is seen that the results given by the isogeometric formulation are slightly lower than the analytical solution [62], however the errors are less than 5%. We observe that the isogeometric results are stable in both a closed-circuit condition and an open-circuit condition similarly to the analytical solution [62], while those of Refs. [61,29] are very different for a closed-circuit condition and an open-circuit condition. The better performance of NURBS-based IGA over the conventional FE method in the solution of the eigenvalue problem is well known and has recently been further addressed in a comprehensive study [63]. Moreover, Table 2 shows that the results obtained using cubic and quartic elements coincide (for the chosen mesh), which suggests the use of cubic element. Furthermore, the convergence of

Table 2
Dimensionless first natural frequency of the simply supported square piezoelectric composite plate [*pie*/0/90/0/*pie*].

Method	Meshing	Degrees of freedom (DOFs)	$\bar{f} = \omega_1 a^2/(10,000t\sqrt{\rho})$	
			Closed circuit	Open circuit
IGA (p = 2) (5 dofs per control point)	8 × 8	500	235.900	236.100
IGA (p = 3) (5 dofs per control point)	8 × 8	605	235.100	235.300
IGA (p = 4) (5 dofs per control point)	8 × 8	720	235.100	235.300
FE layerwise [61]	12 × 12	2208	234.533	256.765
Q9 – HSDT (11 dofs per node) [29]	–	–	230.461	250.597
Q9 – FSDT (5 dofs per node) [29]	–	–	206.304	245.349
Ref. [62]			245.941	245.942

Table 3
Convergence of five first natural frequencies of the square piezoelectric composite plate [*pie*/0/90/0/*pie*].

Meshing	Method	Mode sequence number				
		Mode 1	Mode 2	Mode 3	Mode 4	Mode 5
Open circuit						
5 × 5	IGA (p = 2)	240.100	600.600	750.400	1027.500	1537.800
	IGA (p = 3)	235.700	535.200	685.500	940.700	1137.591
	FE layerwise [61]	276.185	–	–	–	–
9 × 9	IGA (p = 2)	235.800	537.300	686.900	942.700	1095.302
	IGA (p = 3)	235.300	529.000	680.400	933.300	1038.290
	FE layerwise [61]	261.703	–	–	–	–
13 × 13	IGA (p = 2)	235.300	530.500	681.500	934.900	1047.801
	IGA (p = 3)	235.200	528.600	680.100	932.800	1035.791
	FE layerwise [61]	259.655	–	–	–	–
	Q9 – HSDT (11 dofs per node) [29]	250.497	583.185	695.697	980.361	1145.410
	Q9 – FSDT (5 dofs per node) [29]	245.349	558.988	694.196	962.017	1093.010
	Ref. [62]	245.942	–	–	–	–
Close circuit						
5 × 5	IGA (p = 2)	239.500	599.000	749.200	1025.500	1535.101
	IGA (p = 3)	235.100	533.700	684.300	938.800	1134.900
	FE layerwise [61]	249.860	–	–	–	–
9 × 9	IGA (p = 2)	235.600	536.800	686.600	942.000	1094.402
	IGA (p = 3)	235.100	528.500	680.000	932.600	1037.300
	FE layerwise [61]	236.833	–	–	–	–
13 × 13	IGA (p = 2)	235.200	530.200	681.3	934.500	1047.302
	IGA (p = 3)	235.100	528.400	679.9	932.400	1035.301
	FE layerwise [61]	234.533				
	Q9 – HSDT (11 dofs per node) [29]	230.461	520.384	662.915	908.459	1022.091
	Q9 – FSDT (5 dofs per node) [29]	206.304	519.444	663.336	907.636	1020.101
	Ref. [62]	245.941	–	–	–	–

the first five natural frequencies with meshing of 5×5, 9×9 and 13×13 for a closed-circuit condition and an open-circuit condition is displayed in Table 3. Again, it can be seen that the isogeometric results do not vary between closed- and open-circuit conditions, unlike those of the FE layerwise approach in Ref. [61].

Finally, Fig. 4 plots the shape of the first six eigenmodes. It is seen that these shapes reflect correctly the physical modes of the piezoelectric composite plates as given by the analytical solution.

4.2. Static analysis of piezoelectric composite plates

4.2.1. A piezoelectric bimorph beam

We now consider a piezoelectric bimorph beam with the geometry, thickness and boundary condition illustrated in Fig. 5. The beam consists of two identical PVDF uniaxial beams with opposite polarities. The cantilever beam is modeled by five identical plate elements. Each element has dimensions $20 \times 5 \times 1$ mm as shown in Fig. 5. The material properties of PVDF are given in Table 1.

Table 4 contains the deflections of the piezoelectric bimorph beam at the specified control points (for IGA) or nodes (for the conventional FE method) with meshing of 101×6 when a unit voltage (1 V) is applied across the thickness of the beam. It is seen that the present results match well the analytical solution [16] and agree very well with those presented in Refs. [23,19,21] (which are however less accurate). When the order of the basis functions is increased, the accuracy improves and results coincide (for the shown number of digits) with those of the analytical solution [16].

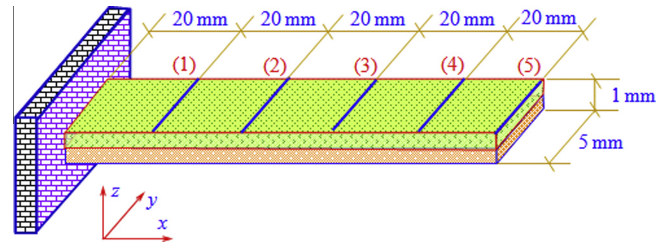

Fig. 5. Geometry of a piezoelectric PVDF bimorph beam.

Table 4
Static deflection of the bimorph piezoelectric beam at various locations ($\times 10^{-6}$ m).

Method	Position				
	1	2	3	4	5
IGA ($p = 2$)	0.0138	0.0550	0.1236	0.2201	0.3443
IGA ($p = 3$)	0.0140	0.0552	0.1242	0.2207	0.3448
EFG [23]	0.0142	0.0555	0.1153	0.2180	0.3416
3D FE [19]	0.0136	0.0546	0.1232	0.2193	0.3410
RPIM [21]	0.0136	0.0547	0.1234	0.2196	0.3435
Analytical solution [16]	0.0140	0.0552	0.1224	0.2208	0.3451

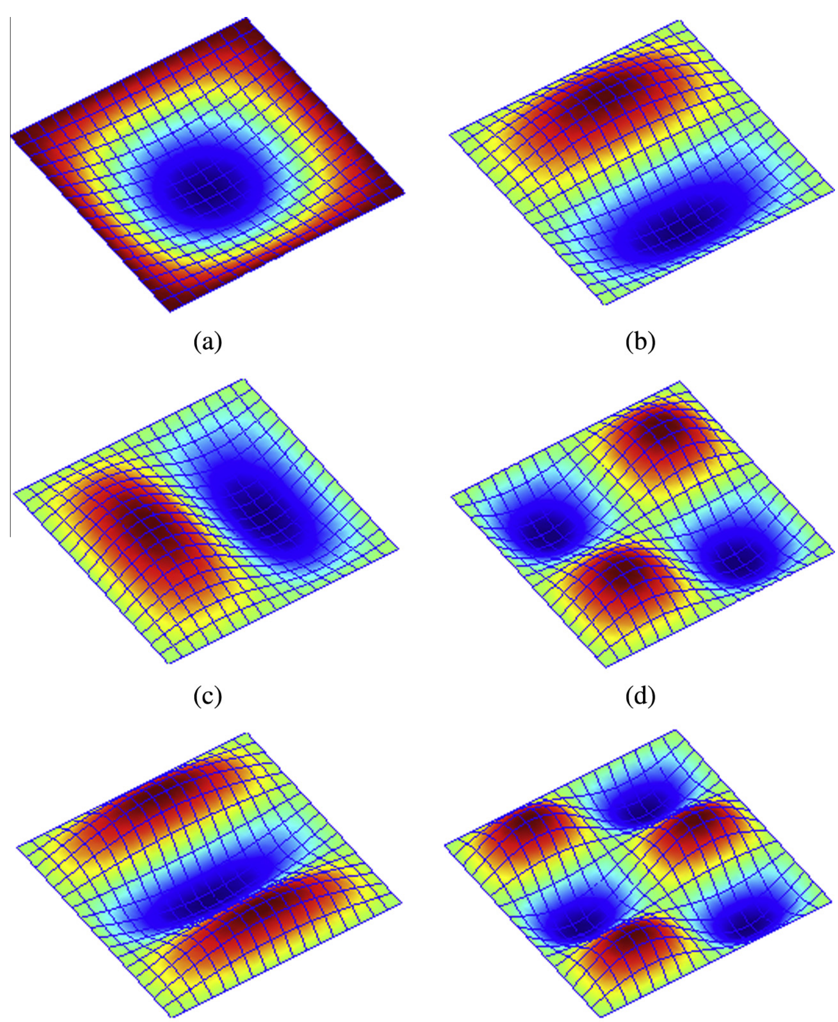

Fig. 4. Shape of the first six eigenmodes of a simply supported piezoelectric composite plate; (a) Mode 1; (b) Mode 2; (c) Mode 3; (d) Mode 4; (e) Mode 5; and (f) Mode 6.

Table 5 reports the tip deflection of the piezoelectric bimorph beam with different input voltages. Again, results obtained with the isogeometric formulation match well the analytical solution [16]. Finally, Fig. 6 shows the effect of the input voltage on the deflection of the piezoelectric bimorph beam. It is observed that when the input voltage becomes larger, the deflection of beam also becomes larger, as expected.

Table 5
Tip deflection of the piezoelectric bimorph beam with different input voltages ($\times 10^{-4}$ m).

Method	Input voltage			
	50 V	100 V	150 V	200 V
IGA ($p = 2$)	0.1721	0.3443	0.5164	0.6885
IGA ($p = 3$)	0.1724	0.3448	0.5173	0.6897
Analytical solution [16]	0.1725	0.3451	0.5175	0.6900

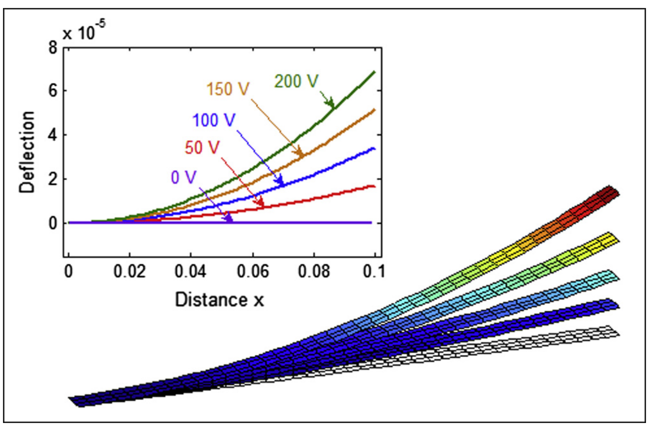

Fig. 6. Deformed shape and centerline deflection of a piezoelectric bimorph beam under different input voltages.

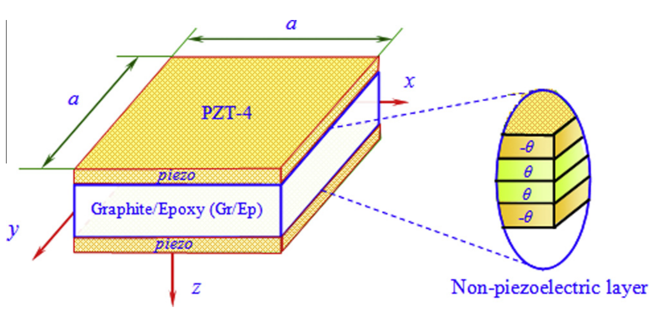

Fig. 7. Square piezoelectric composite plate model.

4.2.2. A piezoelectric composite plate

We now consider a simply supported square laminated plate (20 cm $\times$ 20 cm) subjected to a uniform load $q = 100\,\text{N/m}^2$ as shown in Fig. 7. The plate is bonded by piezoelectric ceramics in both the upper and lower surfaces symmetrically. The plate consists of four composite layers and two outer piezo-layers denoted by *pie*. The laminate configuration of the composite plate is $[pie/-\theta/\theta]_s$ and $[pie/-\theta/\theta]_{as}$ in which subscripts "*s*" and "*as*" indicate symmetric and anti-symmetric laminates, respectively, and θ is the fiber orientation angle of the layers. The thickness of the non-piezoelectric composite plate is 1 mm and each layer has the same thickness. The thickness of the piezo-layer is 0.1 mm. The plate is made of T300/976 graphite/epoxy layers and the piezoceramic is PZTG1195N with their material properties given in Table 1.

Table 6 reports the central point deflection of the simply supported piezoelectric composite plate subjected to the uniform load and different input voltages. Again, the results by the IGA agree well with those of Refs. [21,25]. In addition, Fig. 8 shows the centerline deflection. Four configurations of the composite plate with different fiber orientation angles are investigated including $[pie/-15/15]_{as}$, $[pie/-30/30]_{as}$, $[pie/-45/45]_{as}$ and $[pie/-45/45]_s$. As expected the deflection decreases for increasing input voltage. The reason is that the input voltage induces an upward deflection of the plate due to the piezoelectric effect. This upward contribution becomes prevalent for an input voltage of 10 V. Similar results were obtained in Refs. [21,25].

4.3. Dynamic vibration control analysis of piezoelectric composite plates

4.3.1. A simply supported square plate

We now consider a piezoelectric composite plate subjected to a uniform load $q = 100\,\text{N/m}^2$ with the geometry, boundary conditions and material properties specified in Section 4.2.2. The plate consists of four composite layers and two outer piezoelectric layers denoted by *pie*. The upper and lower surfaces of plate are bonded to a piezoelectric actuator layer and to a piezoelectric sensor layer, respectively. The stacking sequence of the composite plate is $[pie/-45/45]_s$.

First, we study the control of the static deflection. Fig. 9 shows the effect of the displacement feedback control gain G_d on the static deflection of the plate. It is seen that when the displacement feedback control gain G_d becomes bigger, the deflections become

Table 6
Central control point/node deflection of the simply supported piezoelectric composite plate subjected to a uniform load and different input voltages ($\times 10^{-4}$ m).

Input voltage	Scheme	Method			
		CS-DSG3 [25]	RPIM [21]	IGA ($p = 2$)	IGA ($p = 3$)
0 V	$[pie/-45/45]_s$	−0.6326	−0.6038	−0.6343	−0.6375
	$[pie/-45/45]_{as}$	−0.6323	−0.6217	−0.6217	−0.6239
	$[pie/-30/30]_{as}$	−0.6688	−0.6542	−0.6593	−0.6617
	$[pie/-15/15]_{as}$	−0.7442	−0.7222	−0.7422	−0.7452
5 V	$[pie/-45/45]_s$	−0.2863	−0.2717	−0.2799	−0.2842
	$[pie/-45/45]_{as}$	−0.2801	−0.2717	−0.2773	−0.2817
	$[pie/-30/30]_{as}$	−0.2957	−0.2862	−0.2923	−0.2968
	$[pie/-15/15]_{as}$	−0.3259	−0.3134	−0.3233	−0.3283
10 V	$[pie/-45/45]_s$	0.0721	0.0757	0.0745	0.0691
	$[pie/-45/45]_{as}$	0.0601	0.0604	0.0672	0.0606
	$[pie/-30/30]_{as}$	0.0774	0.0819	0.0749	0.0682
	$[pie/-15/15]_{as}$	0.0924	0.0954	0.0957	0.0886

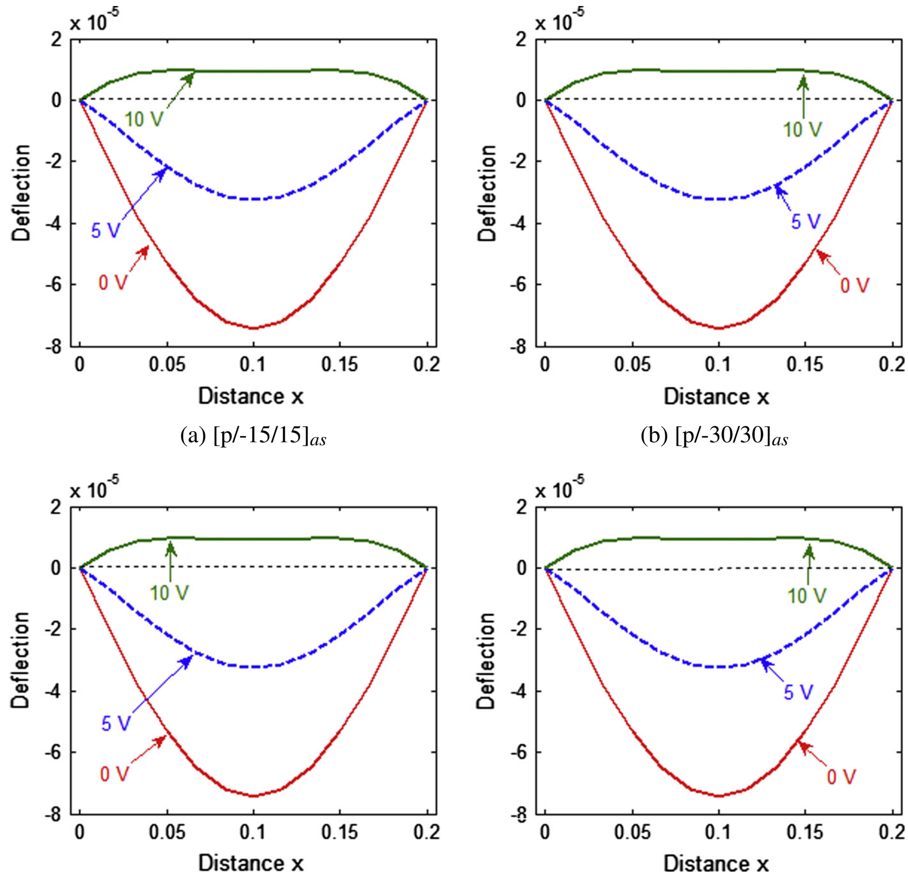

(a) $[p/-15/15]_{as}$ (b) $[p/-30/30]_{as}$ (c) $[p/-45/45]_{as}$ (d) $[p/-45/45]_{s}$

Fig. 8. Centerline deflection of a simply supported piezoelectric composite plate subjected a uniform load and different input voltages.

smaller, similarly to what illustrated in [21]. The reason is that, when the plate is deformed by the external load, electric charges are generated in the sensor layer and amplified through the closed-loop control. The converted signal is then sent to the distributed actuator and an input voltage for the actuator is generated. A resultant force is generated through the converse piezoelectric effect and actively controls the static response of the laminated plate.

Next, the plate is assumed to be subjected to a harmonic load $F = \sin(\bar{\omega}t)$ applied at its central point, where $\bar{\omega}$ is chose to be the first natural angular frequency (ω_1) of the plate. The eigenvalue problem is first solved with a mesh of 13×13 cubic B-spline elements and a value of $\omega_1 = 167.34$ Hz is determined. Fig. 10 shows the transient responses of the center point of the piezoelectric composite plate with and without the velocity feedback gain. It

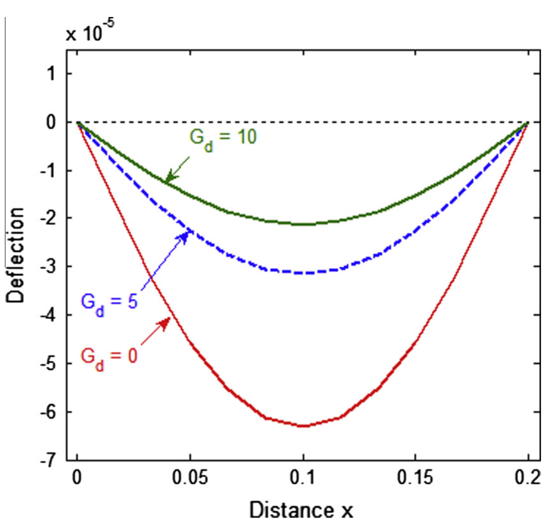

Fig. 9. Effect of the displacement feedback control gain G_d on static deflection of a simply supported piezoelectric composite plate subjected to a uniform load.

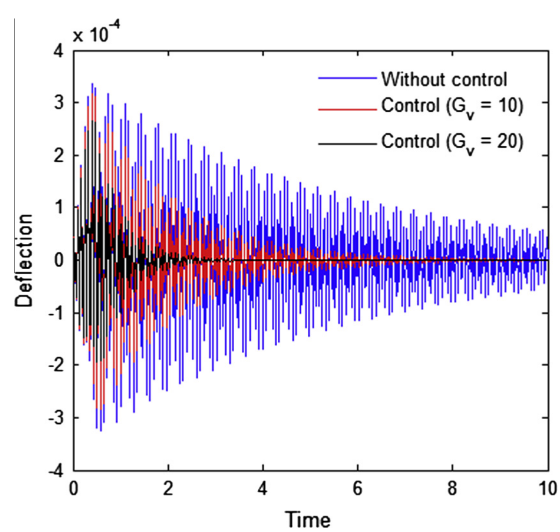

Fig. 10. Effect of the velocity feedback control gain G_v on the dynamic deflection response of a simply supported piezoelectric composite plate subjected to a uniform load.

Please cite this article in press as: P. Phung-Van et al., Comput. Mater. Sci. (2014), http://dx.doi.org/10.1016/j.commatsci.2014.04.068

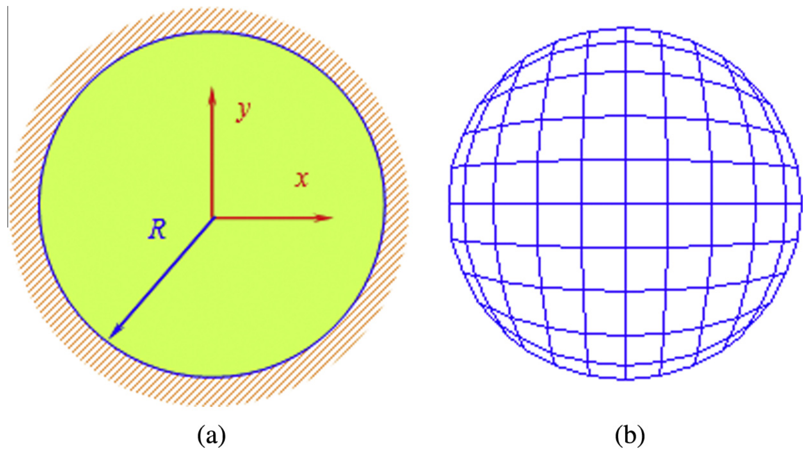

Fig. 11. (a) Circular piezoelectric composite plate model and (b) meshing of 8 × 8 cubic elements.

can be seen that when the gain G_v is equal to zero (without control), the response decreases in time due to the structural damping. By increasing the velocity feedback gain, the transient response is further attenuated and the amplitude of the center point deflection decreases faster, as expected. This is due to an increase of the active damping as per Eq. (37).

4.3.2. A clamped circular plate

In this example, we consider a five-layer ($pie/-45/45/-45/pie$) clamped circular plate of radius R = 5 dm subjected to a harmonic point load $F = \bar{\omega}e^{i\bar{\omega}t}$ at the central point (Fig. 11a). The plate is made of T300/976 graphite/epoxy layers and the piezoceramic is PZTG1195N. The thickness of the non-piezoelectric composite plate is 0.03 dm and each layer has the same thickness, the thickness of the piezo-layer is 0.005 dm. The first natural frequency of plate is calculated with a mesh of 8 × 8 cubic elements (Fig. 11b) and is equal to 113.35 Hz. The effect of the frequency of the applied force history on the deflection of the center of the plate is investigated. $\bar{\omega}$ is changed from 80 to 150, a range including the first natural angular frequency of the structure. The deflection response measured also at the center of the plate is shown in Fig. 12. It is seen clearly that the peak of the response occurs exactly at the value of the first eigenfrequency. Moreover, the deflection at the center point of the plate decreases by applying control, as expected.

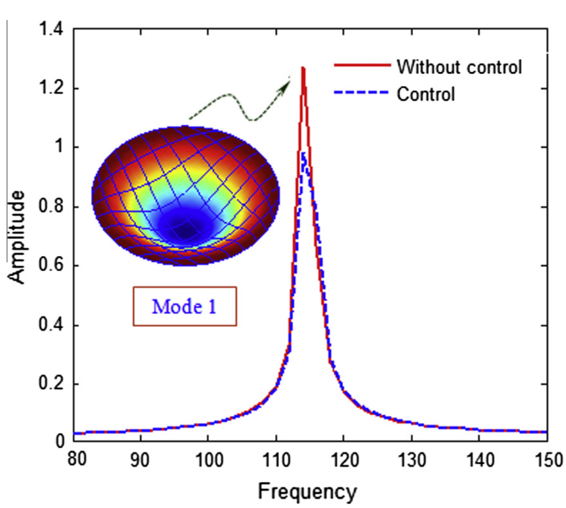

Fig. 12. Dynamic deflection response of a clamped circular plate under a harmonic point load.

5. Conclusions

This paper presents a simple and effective approach based on the combination of IGA and HSDT for the static, free vibration analyses and dynamic control of composite plates integrated with piezoelectric sensors and actuators. In the piezoelectric composite plates, the mechanical displacement field is approximated according to the HSDT using isogeometric elements based on NURBS and featuring at least C^1-continuity, whereas the electric potential is assumed to vary linearly through the thickness for each piezoelectric sub-layer. A displacement and velocity feedback control algorithm is used for the active control of the static deflection and of the dynamic response of the plates through a closed-loop control with bonded or embedded distributed piezoelectric sensors and actuators. Several numerical examples are performed to analyze the static deflection, natural vibration mode and dynamic control of piezoelectric laminated plates with different stacking schemes. Through the presented formulation and numerical results, the following main conclusions can be drawn:

(i) Due to the use of the HSDT, the proposed method does not require shear correction factors. The use of NURBS elements of at least second order naturally fulfills the C^1-continuity requirement of the HSDT, thereby significantly reducing the number of degrees of freedom per control point over conventional finite element approaches featuring C^0 inter-element continuity.
(ii) In free vibration analyses, the predictions of the proposed approach agree well with analytical solutions, and are more stable (passing from closed- to open-circuit conditions) than those of several other approaches available in the literature.
(iii) In static analyses, the predictions of the proposed approach are more accurate than those of several other approaches with a lower number of degrees of freedom.
(iv) In dynamic control analyses, the proposed approach delivers predictions which appear reasonable and consistent with the observed physical behavior.

Acknowledgments

Phung Van Phuc would like to acknowledge the support from the VLIR-OUS scholarship program (Short Research Stays - SRS). L. De Lorenzis would like to acknowledge the support from the Italian MIUR through the project FIRB Futuro in Ricerca 2010 “Structural mechanics models for renewable energy applications” (RBFR107AKG).

References

[1] Z. Wang, S. Chen, W. Han, Finite Elem. Anal. Des. 26 (1997) 303–314.
[2] S.M. Yang, Y.J. Lee, Smart Mater. Struct. 3 (1994) 494–500.
[3] [3] B. Pletner, H. Abramovich, AIAA J. 35 (1997) 1316–1326.
[4] C.H. Hong, I. Chopra, AIAA J. 37 (1999) 372–377.
[5] J. Kim, V.V. Varadan, V.K. Varadan, X.Q. Bao, Smart Mater. Struct. 5 (1996) 165–170.
[6] C. Willberg, U. Gabbert, Acta Mech. 223 (8) (2012) 1837–1850.
[7] K.Y. Lam, X.Q. Peng, G.R. Liu, J.N. Reddy, Smart Mater. Struct. 6 (1997) 583–591.
[8] A. Benjeddou, Comput. Struct. 76 (2000) 347–363.
[9] H. Allik, T.J.R. Hughes, Int. J. Numer. Meth. Eng. 2 (1970) 151–157.
[10] K. Kekana, J. Sound Vib. 256 (2002) 463–473.
[11] S.Y. Wang, Int. J. Solids Struct. 41 (2004) 4075–4096.
[12] D.K. Cheng, Field and Wave Electromagnetics, second ed., Addison-Wesley Publishing, 1989.
[13] S.M. Ehlers, T.A. Weisshaar, AIAA J. 28 (1990) 1611–1623.
[14] S.Y. Wang, S.T. Quek, J. Intell. Mater. Syst. Struct. 13 (2002) 61–70.
[15] S.Y. Wang, S.T. Quek, K.K. Ang, Smart Mater. Struct. 10 (2001) 637–644.
[16] A. Suleman, V.B. Venkayya, J. Intell. Mater. Syst. Struct. 6 (1995). 776–782.
[17] T. Bailey, J.E. Hubbard, J. Guid. Control Dyn. 8 (1985) 605–611.
[18] I.Y. Shen, Smart Mater. Struct. 4 (1995) 340–355.
[19] H.S. Tzou, C.I. Tseng, J. Sound Vib. 138 (1990) 17–34.
[20] W.C. Hwang, H.C. Park, AIAA J. 31 (1993) 930–937.
[21] G.R. Liu, K.Y. Dai, K.M. Lim, Smart Mater. Struct. 13 (2004) 1438–1447.
[22] G.R. Liu, X.Q. Peng, K.Y. Lam, J. Tani, J. Sound Vib. 220 (1999) 827–846.
[23] K.M. Liew, H.K. Lim, M.J. Tan, X.Q. He, Comput. Mech. 29 (2002) 486–497.
[24] A. Milazzo, C. Orlando, Smart Mater. Struct. 21 (2012) 075031.
[25] P. Phung-Van, T. Nguyen-Thoi, T. Le-Dinh, H. Nguyen-Xuan, Smart Mater. Struct. 22 (2013) 095026.
[26] A.A. Khdeir, O.J. Aldraihem, Smart Mater. Struct. 20 (2011) 105030.
[27] R.S. Kumar, M.C. Ray, Int. J. Mech. Mater. Des. 8 (2012) 197–218.
[28] M. Rezaiee-Pajand, Y. Sadeghi, Latin Am. J. Solids Struct. 10 (2013) 323–348.
[29] M.F.C. Victor, A.A.G. Maria, S. Afzal, M.M.S. Cristóvão, A.M.S. Carlos, C.V.M. Franco, Comput. Methods Appl. Mech. Eng. 185 (2000) 325–346.
[30] J.A. Mitchell, J.N. Reddy, Int. J. Solids Struct. 32 (1995) 2345–2367.
[31] J.N. Reddy, Eng. Struct. 21 (1999) 568–593.
[32] T.J.R. Hughes, J.A. Cottrell, Y. Bazilevs, Comput. Methods Appl. Mech. Eng. 194 (39–41) (2005) 4135–4195.
[33] J.A. Cottrell, T.J.R. Hughes, Y. Bazilevs, Isogeometric Analysis, Towards Integration of CAD and FEA, Wiley, 2009.
[34] F. Amiri, D. Milan, Y. Shen, T. Rabczuk, M. Arroyo, Theoret. Appl. Fract. Mech. 69 (2014) 102–109.
[35] T. Rabczuk, P.M.A. Areias, T. Belytschko, Int. J. Numer. Meth. Eng. 72 (5) (2007) 524–548.
[36] T. Rabczuk, P.M.A. Areias, CMES-Comput. Model. Eng. Sci. 16 (2) (2006) 115–130.
[37] P. Areias, T. Rabczuk, Int. J. Numer. Meth. Eng. 94 (12) (2013) 1099–1122.
[38] T. Chau-Dinh, G. Zi, P.S. Lee, J.H. Song, T. Rabczuk, Comput. Struct. 92–93 (2012) 242–256.
[39] N. Vu-Bac, H. Nguyen-Xuan, L. Chen, S. Bordas, P. Kerfriden, R.N. Simpson, G.R. Liu, T. Rabczuk, Comput. Model. Eng. Sci. 73 (4) (2011) 331–355.
[40] N. Vu-Bac, H. Nguyen-Xuan, L. Chen, C.K. Lee, G. Zi, X. Zhuang, G.R. Liu, T. Rabczuk, J. Appl. Math. 2013 (2013) 978026.
[41] P. Areias, T. Rabczuk, D. Dias-da-Costa, Finite Elem. Anal. Des. 66 (2013) 53–67.
[42] P. Areias, T. Rabczuk, D. Dias-da-Costa, CMES-Comput. Model. Eng. Sci. 88 (6) (2012) 475–506.
[43] S.S. Nanthakumar, T. Lahmer, T. Rabczuk, Int. J. Numer. Meth. Eng. 96 (2013) 373–389.
[44] H. Nguyen-Vinh, I. Bakar, M.A. Msekh, J.H. Song, J. Muthu, G. Zi, P. Le, S. Bordas, R. Simpson, S. Natararajan, T. Lahmer, T. Rabczuk, Eng. Fract. Mech. 92 (2012) 19–31.
[45] C. Thai-Hoang, N. Nguyen-Thanh, H. Nguyen-Xuan, T. Rabczuk, Appl. Math. Comput. 217 (17) (2011) 7324–7348.
[46] H.H. Phan-Dao, H. Nguyen-Xuan, C. Thai-Hoang, T. Nguyen-Thoi, T. Rabczuk, Int. J. Comput. Methods 10 (1) (2013) 1340005.
[47] X. Zhuang, R. Huang, H. Zhu, H. Askes, K. Mathisen, Finite Elem. Anal. Des. 75 (2013) 1–7.
[48] T. Rabczuk, R. Gracie, J.H. Song, T. Belytschko, Int. J. Numer. Meth. Eng. 81 (1) (2010) 48–71.
[49] J.A. Cottrell, A. Reali, Y. Bazilevs, T.J.R. Hughes, Comput. Methods Appl. Mech. Eng. 195 (41–43) (2006) 5257–5296.
[50] D.J. Benson, Y. Bazilevs, M.C. Hsu, T.J.R. Hughes, Comput. Methods Appl. Mech. Eng. 199 (5–8) (2006) 276–289.
[51] J. Kiendl, K.Y. Bletzinger, J. Linhard, R. Wchner, Comput. Methods Appl. Mech. Eng. 198 (49–52) (2006) 3902–3914.
[52] W.A. Wall, M.A. Frenzel, C. Cyron, Comput. Methods Appl. Mech. Eng. 197 (33–40) (2008) 2976–2988.
[53] Chien H. Thai, H. Nguyen-Xuan, N. Nguyen-Thanh, T.H. Le, T. Nguyen-Thoi, T. Rabczuk, Int. J. Numer. Meth. Eng. 91 (6) (2012) 571–603.
[54] Chien H. Thai, A.J.M. Ferreira, S.P.A. Bordas, T. Rabczuk, H. Nguyen-Xuan, Eur. J. Mech. A. Solids 43 (2014) 89–108.
[55] N. Valizadeh, S. Natarajan, O.A. Gonzalez-Estrada, T. Rabczuk, T.Q. Bui, S.P.A. Bordas, Compos. Struct. 99 (2013) 309–326.
[56] H. Ghasemi, R. Brighenti, X. Zhuang, J. Muthu, T. Rabczuk, Comput. Mater. Sci. 83 (2014) 463–473.
[57] Loc V. Tran, Thai H. Chien, H. Nguyen-Xuan, Finite Elem. Anal. Des. 73 (2013) 65–76.
[58] N. Nguyen-Thanh, J. Kiendl, H. Nguyen-Xuan, R. Wüchner, K.U. Bletzinger, Y. Bazilevs, T. Rabczuk, Comput. Methods Appl. Mech. Eng. 200 (47–48) (2011) 3410–3424.
[59] J.M. Reddy, J. Appl. Mech. 51 (1984) 745–752.
[60] J.N. Reddy, Mechanics of Laminated Composite Plates – Theory and Analysis, CRC Press, New York, 1997.
[61] D.A. Saravanos, P.R. Heyliger, D.A. Hopkins, Int. J. Solids Struct. 34 (1997) 359–378.
[62] P. Heyliger, D.A. Saravanos, J. Acoust. Soc. Am. 98 (1995) 1547–1557.
[63] T.J.R. Hughes, J.A. Evans, A. Reali, Comput. Methods Appl. Mech. Eng. 272 (2014) 290–320.

Please cite this article in press as: P. Phung-Van et al., Comput. Mater. Sci. (2014), http://dx.doi.org/10.1016/j.commatsci.2014.04.068